VIP Cluster-Assembled Materials Very Important Paper

Deutsche Ausgabe: DOI: 10.1002/ange.201507237
Internationale Ausgabe: DOI: 10.1002/anie.201507237

A Filled-Honeycomb-Structured Crystal Formed by Self-Assembly of a Janus Polyoxometalate–Silsesquioxane (POM–POSS) Co-Cluster

Chi Ma, Han Wu, Zi-Han Huang, Ruo-Hai Guo, Min-Biao Hu, Christian Kübel, Li-Tang Yan,* and Wei Wang**

Abstract: *Clusters with diverse structures and functions have been used to create novel cluster-assembled materials (CAMs). Understanding their self-assembly process is a prerequisite to optimize their structure and function. Herein, two kinds of unlike organo-functionalized inorganic clusters are covalently linked by a short organic tether to form a dumbbell-shaped Janus co-cluster. In a mixed solvent of acetonitrile and water, it self-assembles into a crystal with a honeycomb superstructure constructed by hexagonal close-packed cylinders of the smaller cluster and an orderly arranged framework of the larger cluster. Reconstruction of these structural features via coarse-grained molecular simulations demonstrates that the cluster crystallization and the nanoscale phase separation between the two incompatible clusters synergistically result in the unique nano-architecture. Overall, this work opens up new opportunities for generating novel CAMs for advanced future applications.*

The past decades have witnessed significant progress in building complex nano-architectures by exploiting self-assembly of versatile building blocks.[1–3] The achievements are based on understanding the fundamental principles governing the formation and growth of self-assembled nano-architectures, that is, transitions between disordered and ordered states. Consequently, we can tailor the self-assembly process by modulating the ordering phenomena through manipulation of the intermolecular non-covalent interactions between rationally designed building blocks. In this respect, crystallization of nanoparticles is one good example.[4–8] Like atoms, nanoparticles can crystalize into colloidal crystals in which nanoparticles occupy the lattice points of superlattices.[4–6] Furthermore, the structural diversity of superlattices has been well explored for colloidal alloys of binary nanoparticles.[7,8] These ordered structures are expected to play vital roles in future electronic and optoelectronic applications.[9] Another good example is the disorder-to-order transition of block copolymers.[10–14] During the transition, incompatible blocks microphase-separate into periodic morphologies in which orderly arranged phase-separated domains of one component are embedded in a continuous matrix of the other component. The diversity of morphologies ranges from spheres to cylinders to lamellae as a function of volume fraction, which have been used to fabricate functional materials and devices.[15] Right now, a fundamental challenge is how to exploit the various transitions to tailor the mechanism of the self-assembly process to generate new nano-architectures.

Nanoscale clusters are atomically precise ensembles of bound atoms with sizes intermediate between molecules and bulk solids. They exhibit an amazing diversity in structure, chemical composition, shape, and functionality. Their properties enable them to be used as novel building blocks in the design and construction of emerging cluster-assembled materials (CAMs) which have well-defined structures and desired functions.[16] Most clusters can crystallize, but cannot form co-crystals with other clusters mainly because of differences in their structures and properties.[17–19] This situation means that it is difficult to guide incompatible clusters to form predesigned structures with desired performance, thus the development of CAMs is greatly limited. To overcome these difficulties, Janus particles[20–22] and co-clusters[23,24] have been devised with a desire to boost the development of novel CAMs with expected properties and diverse structures. The approach is implemented by covalently linking two different types of clusters forming Janus particles or co-clusters to avoid macroscopic phase separation. With carefully selected clusters and rationally designed co-clusters, they will exhibit dual characteristics, that is, they might synergistically self-assemble into novel nano-architectures by taking full advantage of two ordering phenomena: cluster crystallization and nanoscale phase separation of the two incompatible blocks.

Herein, we designed and synthesized an A–B co-cluster composed of two different types of organo-functionalized inorganic clusters (Figure 1 a).[23] Cluster A is a complex of a Wells-Dawson-type polyoxometalate (POM) anion $(P_2W_{15}V_3O_{62})^{9-}$ with its counterions: six tetrabutylammonium (TBA, Bu_4N^+) surfactant cations and three protons (H^+).[25] (For simplification, the POM-ligand complex is denoted as "POM cluster" hereafter.) The molecular weight of the

[*] C. Ma,[+] H. Wu,[+] Dr. M.-B. Hu, Prof. Dr. W. Wang
Center for Synthetic Soft Materials, Key Laboratory of Functional Polymer Materials of Ministry of Education and Institute of Polymer Chemistry, Collaborative Innovation Center of Chemical Science and Engineering (Tianjin), Nankai University
Tianjin, 300071 (P. R. China)
E-mail: weiwang@nankai.edu.cn

Z.-H. Huang,[+] Dr. R.-H. Guo, Prof. Dr. L. T. Yan
Department of Chemical Engineering, Tsinghua University
Beijing, 100084 (P. R. China)
E-mail: ltyan@mail.tsinghua.edu.cn

Dr. C. Kübel
Karlsruhe Nano Micro Facility and Institute of Nanotechnology
Hermann-von-Helmholtz-Platz 1, 76344
Eggenstein-Leopoldshafen (Germany)
E-mail: christian.kuebel@kit.edu

[+] These authors contributed equally to this work.

Supporting information for this article is available on the WWW under http://dx.doi.org/10.1002/anie.201507237.

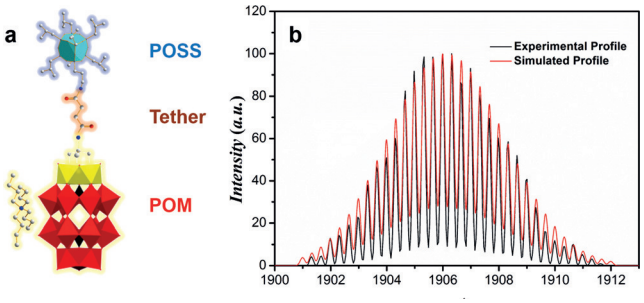

Figure 1. a) Dumbbell-shaped molecule composed of a POM cluster and a POSS cluster covalently linked by a short organic tether. b) Experimental and simulated isotopic distribution patterns, selected from the co-cluster ESI-MS spectrum, corresponding to $[POSS\text{-}C_4\text{-}POM^{6-} + 3TBA^{+}]^{3-}$.

complex is 5422 Da and the POM core has an ellipsoidal shape with a long axis of about 1.2 nm and a short axis of about 1.0 nm. Cluster B is an aminopropylisobutyl derivative of polyhedral oligomeric silsesquioxanes (POSS). In this cubic cage, seven isobutyl groups are attached to seven corners and an aminopropyl group is attached to the eighth corner. Its molecular weight is 874 Da and it has a spherical shape with a diameter of approximately 1.3 nm when all the isobutyl groups are fully extended.[26,27] The POM–POSS co-cluster is constructed by covalently linking the POM cluster and the POSS cluster together via a short organic tether (ca. 1.0 nm). The length of the co-cluster was estimated to be 3.5 nm for the fully extended configuration based on the single-crystal data[36] of Tris-derived Wells-Dawson POM, octa-isobutyl-POSS and succinic acid with the aid of Chem-Bio3D. The full electrospray ionization mass spectrum is shown in Figure S1 in the Supporting Information, and a clear assignment of all the mass peaks is in Table S1. In Figure 1b the peak in an isotopic envelope is at a mass-to-charge ratio of m/z 1906.00 corresponding to $[POSS\text{-}C_4\text{-}POM^{6-} + 3TBA^{+}]^{3-}$, agreeing with the simulated value of m/z 1905.99. This indicates that we obtain a 6445 Da molecular weight of the co-cluster. The uniform molecular length and the atomically precise molecular weight are important factors for a precise control of the self-assembled nano-architectures.

Besides these two factors, the spatial structure and properties of this co-cluster are also crucial factors for programming to produce the desired nanostructures. From a structural perspective, the dumbbell shape, formed by two rigid but unlike clusters linked by the short and flexible tether, implies an option for three-dimensional (3D) shape manipulation.[28,29] The rigidity of the clusters provides a strong drive for a brick-like packing of the building blocks, while the flexibility of the tether awards a certain degree of freedom for configuration adjustment of the two unlike clusters to achieve better packing in the space-filling structure.

The Janus characteristic of the co-cluster is reflected in the solubility difference of the two clusters. For instance, the POM cluster dissolves in some polar solvents, such as dimethylformamide, whereas the POSS cluster dissolves well in most nonpolar solvents, such as tetrahydrofuran and toluene. This difference indicates that they are incompatible under the conditions used in this work. Indeed, we observed nanoscale phase-separated lamellar structures with a sub-5 nm periodicity, identical to the lamellar morphology of symmetrical block copolymers, in ultra-thin films (Supporting Information, Figure S2a) and onion-type nanoparticles (Figure S2b). However, ordered structures related to individual clusters were not found within the lamellae.[23,24] Noticeably, these specimens were prepared simply by casting from an acetonitrile solution onto the water surface to form ultra-thin films or by dropping the solution into water to generate nanoparticles. With these approaches, the rapid mixing of acetonitrile and water results in solidification or agglomeration of the co-cluster within a few seconds.

The acetonitrile/water solution of the co-cluster shows a strong Tyndall scattering (Figure S3a). At a 1/9 acetonitrile/water ratio, solid-state crystals of this co-cluster slowly grow at ambient conditions. When their average size is in the range of a few tens to one hundred nanometers we characterized them by electron microscopy (Figure S3b) and found a bimodal distribution (Figure S3c). To reveal their 3D structures, high-angle annular dark-field scanning transmission electron microscopy (HAADF-STEM) imaging together with electron tomographic analysis were used.[30–32] The higher atomic numbers, Z, of tungsten and vanadium in the POM cluster compared to those of silicon and carbon in the POSS cluster and the organic tether allowed us to apply Z-contrast imaging to directly visualize the 3D structure of the segregated POM and POSS clusters. In the Z-contrast images, the POM structures are brighter than the POSS cluster and the organic tether (Figure S4). Using a tilt series of HAADF-STEM images, we created a tomographic reconstruction (Figure 2a and Movies S1 and S2 in the Supporting Information) to visualize the full 3D structure. Almost all of the large crystals analyzed by electron tomography show that the co-cluster self-assembled into hexagonal crystals with a filled honeycomb superstructure constructed by the bright POM framework and the dark POSS domains, while single 2D STEM images show various projections of the hexagonal structure (Figure S4). This indicates the formation of solid-state crystals of the POM-POSS co-cluster with a nanoscale phase separation between the incompatible POM and POSS blocks.

The images (Figure 2b and c) show the 3D structural information obtained by digital slicing of the reconstructed volume. A horizontal slice of the prism in Figure 2b clearly shows one of its hexagonal cross sections. The six red dashed lines outline the six main facets of the prism and the angle between two adjacent facets is approximately 120°. In Figure 2b, we also see hexagonal close-packed POSS domains. A vertical slice in Figure 2c, obtained along cutting direction (CD) in Figure 2a, shows the structure within the vertical section of the prism. The alternating bright and dark strips penetrate the crystal from top to bottom, indicating the formation of POSS cylinders with a fluctuated and hazy boundary between bright and dark strips. These analyses and the tomographic movies (Movies S1 and S2) confirm that the hexagonal close-packed POSS cylinders and the POM framework constitute the honeycomb in the hexagonal crystals (Figure 2d).

Under low-dose conditions individual nanosized POM clusters are recognizable in high-resolution STEM images.

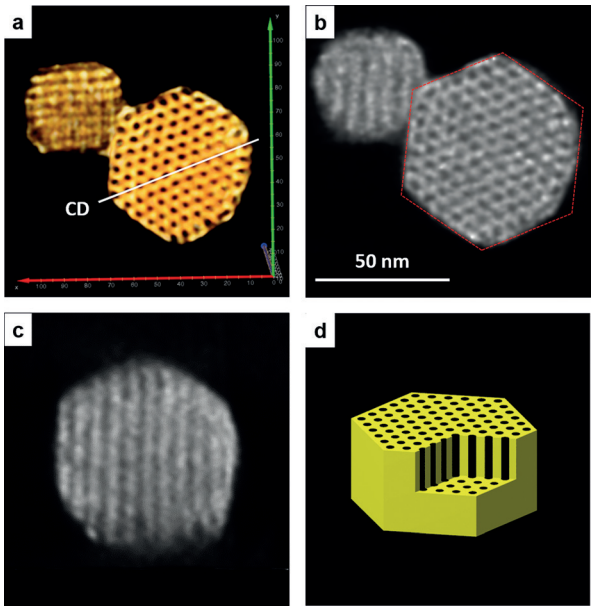

Figure 2. a) Volume rendering of a HAADF-STEM tomographic reconstruction showing a 3D hexagonal crystal with a filled-honeycomb network constructed from a bright POM framework and dark POSS domains. The cutting direction (CD) for perpendicular slices is indicated. b) Horizontal digital slice through the reconstructed volume showing the hexagonal structure. The six dashed lines highlighted the six facets. c) Digital slice obtained in perpendicular direction at CD showing alternating bright and dark columns penetrating the crystal from top to bottom. d) Idealized 3D filled-honeycomb superstructure in the hexagonal crystal (yellow POM, black POSS).

This information is utilized to study the fine structures within the honeycomb crystals. The image (Figure 3a) shows a honeycomb crystal imaged along the hexagonal axis. The distribution and arrangement of the bright POM clusters map the nanostructure in the framework. Clearly, the POM clusters assemble into a bilayer with a uniform thickness of about 2 nm, except for single-POM layers on most of the outmost surfaces of the crystals. A fast Fourier transform (FFT) spot pattern (Figure 3b) corresponds to the hexagonal structure (Figure 3a). The hexagonally arranged FFT spots clearly reveal the average hexagonal symmetry of the self-assembled structure. The planes of the hexagonally arranged cylinders are indexed in Figure 3b and the center-to-center distance separation between the cylinders is $d = 5.4$ nm. The weak spots indicated by the green arrows and the diffusive arc outside of the hexagonal spots are the result of the ordered arrangement of the POM clusters within the bilayer with an average distance of about 1.4 nm between the POM clusters.

In a Fourier filtered close-up image (Figure 3c), the clearly recognizable individual POM clusters enable us to scan their packing and ordering within the bilayer framework. First, a brick-like packing of the POM clusters within the bilayer and an approximately 0.5 nm gap between adjacent POM clusters as a result of the TBA ligands are visible. The arrangement of the POM clusters within the bilayer is not perfect, which results in diffusive arcs in the FFT pattern (Figure 3b). Second, three straight bilayers meet at intersection points to form the framework. The bilayer length between intersection points is approximately equal to the length of four POM clusters or less. Thus, the bilayer growth is interrupted at the intersection points where the position and orientation of the POM clusters changes. Third, individual cells, as outlined by the red lines in Figure 3c, can be distinguished after careful judgment of the linkage of the POM cluster with its POSS partner that is schematically shown by the green dots and tethers (Figure 3c). They are composed of a POSS cylinder encapsulated by a deformed ring of a POM single layer. By counting the member, N_P, of the POM clusters in the sleeve (see the inset of Figure 3d) and plotting N_P as a function of the layer number, N_L, from the outermost layer to the center of this crystal (Figure 3a), we found $10 < N_P < 12$ in $1 \le N_L \le 2$ and $N_P = 10$ in $N_L \ge 3$. This suggests that ten co-clusters come together to construct the most stable cell with an area of 29.3 ± 2.3 nm^2 (Figure S5). $10 < N_P < 12$ in $1 \le N_L \le 2$ means that the cells within the first and second layers are still under construction.

For a further analysis of the packing, we pay close attention to the cross-sectional shape of the cells. It is clear that they do not have a circular shape. We selected six images to show the typical shapes of six cells at $N_P = 10$ (Figure 3e). At first glance, a cell is seemingly formed by four POM layers. When taking into account the POM clusters at intersection points, however, it is more reasonable to describe the shapes of the POM rings as irregular hexagons (or polygons with five to seven sides), as approximately outlined by the red lines with different lengths. Note that the shapes of the six cells and many others (Figure S6) are different from each other to some extent. Meanwhile, the shape of the POSS cylinders is close to rectangular with a length-to-width ratio of 1.38. This value could indicate the packing of the POSS cluster with an aspect ratio of approximant 4:3.

Next, we turn to the cell tessellation or tiling to capture the features of global packing. We selected four images exhibiting four hexagonal arrays of six cells (Figure 3f). The deviation from the regular hexagon increases from top-left to bottom-right. We notice that these irregular hexagon cells, like honeycomb ones, nevertheless organize into a hexagonal array with medium-range order. In a mathematical sense, this organization is a tessellation, that is, a way for these irregular hexagons to build an array with hexagonal symmetry to fill the whole cross-section of the crystal with no gaps and overlaps. Statistically, a regular arrangement of the centers of the irregularly shaped cells is observed, which gives rise to the hexagonal FFT pattern (Figure 3b), suggesting the periodic feature of the cell tessellation, whereas the cell structure of the POSS cylinders wrapped by a deformed POM rings reflects a semi-regular feature of the cell tessellation.

These experimental findings and further analyses evidently demonstrate the synergistic self-assembly of the co-cluster into a hierarchical nano-architecture. All in all, the predetermined structure and unique properties of the co-cluster define the formation of crystals with a filled-honeycomb superstructure. The synergistic effect is reflected by two kinds of ordering phenomena, that is, the phase separation between the incompatible cluster blocks and their crystallization, simultaneously creating the nano-architecture. Clearly, the phase separation results in the hexagonal frame-

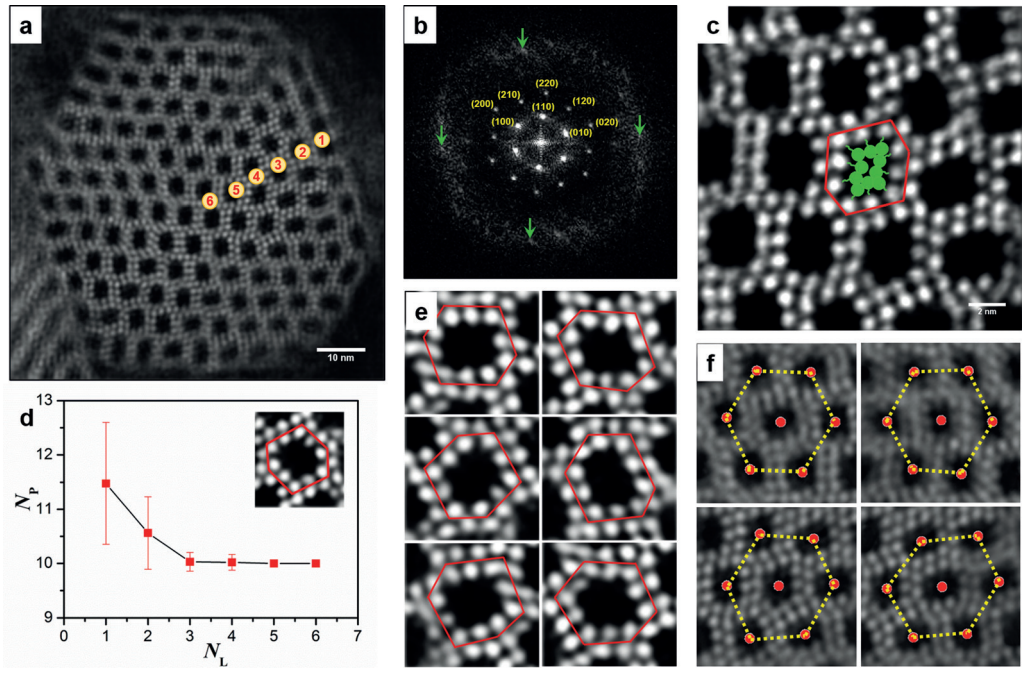

Figure 3. a) Low-dose high-resolution HAADF-STEM image showing the fine structures with a crystal. Scale bar: 10 nm. b) Fast Fourier transform (FFT) spot pattern of the honeycomb crystal. c) Fourier filtered close-up image. A cell, as outlined by six red lines, contains ten clusters. Scale bar: 2 nm. d) The number, N_P, of the POM clusters surrounding a POSS cylinder as a function of the layer number, N_L (numbers 1–6 in (a)), from the outermost layer to the center of this crystal. e) Selected images showing shape deformations of the cell cross sections at $N_P = 10$. f) Selected images showing deviations of the arrangement of the cylinder center from the perfect hexagon. See text for further details to all images.

work of the POM block with the cylinders of the POSS blocks. The crystallization of, at least, the POM cluster causes the ordered packing of the POM cluster within the bilayer. Certainly, POM and POSS act in a cooperative manner to realize the filled-honeycomb-structured crystal.

The fine structure and the shape and tessellation of cells (Figure 3) also reflect the effect of the competition between the two kinds of ordering phenomena on the self-assembled structures. On one hand, the crystallization occurs within a confined space, that is, the POM bilayer framework created by the phase separation. To minimize the free energy, the POM bilayer should grow as long as possible and the POM clusters should arrange as perfectly as possible. On the other hand, simultaneous phase separation, which prefers the formation of hexagonal cylinders, changes the bilayer growing direction, or more precisely speaking, breaks the bilayer. This breakage results in shortened bilayers and imperfect packing at intersection points. The crystallization of the POM cluster in the bilayer framework forces a circular POSS cylinder, which is the preferred packing with minimal interface energy, to convert into an approximately rectangular one. Thus, the competition is responsible for a frustrated structure leading to local variations in the cluster packing and cell shape. Overall, the synergy between the two ordering phenomena cooperatively and competitively results in the cluster packing defects, the cell-shape deformation, and the deviation of the cell arrays. Thus, the deformed cell tessellation features both periodicity and semi-regularity.

To gain an in-depth insight into the underlying mechanism of the experimentally observed hexagonal superstructure, we performed systematic coarse-grained (CG) molecular simulations of the self-assembly of the POM–POSS Janus co-clusters (see Supporting Information for simulation details). The CG model of the co-cluster is presented in Figure 4a, where violet and green beads with different radii, R and r, are utilized to represent the POM and POSS clusters respectively, which are linked by a short tether modeled as chains of two small beads. The values of R and r are selected to mimic the effective volume of POM and POSS clusters, taking both TBA cations and isobutyl chains into account.

The series of simulations reveals that the size asymmetry of the two end group beads has a significant impact on the resulting self-assembled structures. Within the radius ratio, R/r, ranging from 1.5 to 1.8, the co-clusters self-assemble into hexagonal structures similar to that found in the experiments. A careful comparison between the hexagonal structures obtained from experiments and simulations has been made by examining the N_P at different R/r, as demonstrated in Figure 4b. It is evident that N_P decreases in response to the rising R/r, and we find that $N_P \approx 10$ in the shadowed regime of R/r, which is in good agreement with the experiment results (Figure 3d) and a geometrical analysis (Figure S7). The typical hexagonal superstructure that is constructed of a bilayer framework of the violet beads around the cylinders of the green beads is given in Figure 4c, and its 3D features displayed in Movie S3. Just as with Figure 2c, the cylinder structures can be easily identified by a look along the red line in Figure 4c in a perpendicular direction (Figure 4d).

In Figure 4e, the disordered POSS packing in the cylinders is visible. The interface between the cylinders and framework is rough as also experimentally indicated in Figure 2c. The framework of the POM clusters is a typical hexagonally close-packed (HCP) structure according to the simulation results. However, defects can still be found due to the size asymmetry and the confined space that may lead to kinetic trapping during the crystallization and simultaneous phase separation. Indeed, vacancies and dislocations can be found in a three-straight-POM framework (Figure 4f), and

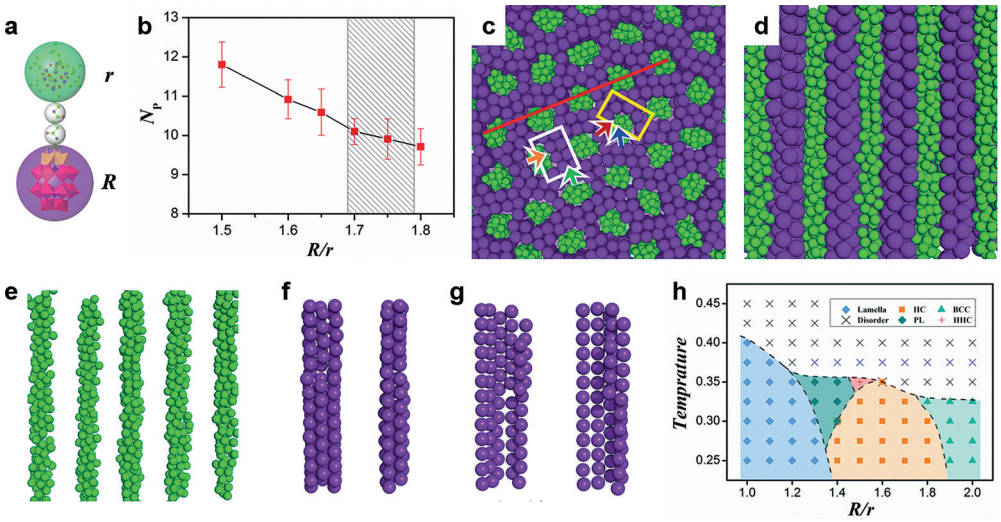

Figure 4. a) Coarse-grained model of the Janus co-clusters used in the simulation. The violet (POM) and green (POSS) beads have different radii, *R* and *r*, and are linked by a short tether modeled as chains of two beads. b) Plot of N_p as a function of *R*/*r* (hatched area: *R*/*r* where $N_p \approx 10$). c) Typical hexagonal superstructure that is constructed by a framework of bilayers of the violet beads with the cylinders of the green beads. d) Slice obtained in the perpendicular direction along the red line in (c) showing the arrangements of the violet and green beads. e) Conformation of the selected five cylinders of the green beads. f) Arrangement of the violet beads in the framework bilayer, in the white rectangle in (c), the orange and green arrows in (c) denote the viewpoints of the left and right structures in (f), respectively. g) Observations of arrangements of the violet beads at an intersection point highlighted by the yellow rectangle in (c) at two directions that are indicated by the two arrows in (c). The left and right arrangements correspond to blue and red arrows (excluding the green beads). h) Phase diagram showing that the co-cluster can self-assemble into lamella (blue diamond), honeycomb (HC; red square), body centered cubic (BCC; green triangle), perforated lamella (PL; green diamond), helix to honeycomb (HHC; red cross) structures, and disorder X.

a body centered cubic (BCC) packed framework (Figure 4g) can be found at the corner of the cell instead of a typical HCP structure. These defects and local variations are probably the reason why it is difficult to get good images (projections) in a direction perpendicular to the hexagonal axis experimentally (Figure S8).

To gain further understanding of the crucial effects of the size asymmetry, a phase diagram with various temperatures and radius ratios, *R*/*r*, is given in Figure 4h. Four main structures, lamella, perforated lamella (PL), honeycomb (HC), and body centered cubic (BCC) spherical micelles are obtained by changing *R*/*r*. All the structures obtained in the phase diagram, including the helix to honeycomb (HHC), are shown in Figure S9. Clearly, the self-assembled structure significantly depends on the value of *R*/*r*, highlighting that the size asymmetry (shape entropy) plays a significant role in the formation of the different superstructures.[33–35]

In summary, covalent linking two unlike organo-functionalized inorganic clusters using a flexible organic tether creates a simple dumbbell-shaped Janus co-cluster. As a result, it possesses asymmetries in size and Janus characteristics with a restricted separation between the unlike clusters. A subtle balance of these factors established simply by solvent tuning results in two kinds of ordering phenomena, that is, crystallization of the same clusters and nanoscale phase separation between the incompatible clusters, to synergistically define the self-assembly of the co-cluster in solution into the crystals with a honeycomb superstructure. The concepts presented herein could be extended to a large number of existing and emerging clusters as well as to nanoparticles for creation of novel cluster- or particle-assembled materials with novel self-assembled superstructures and desired functions.

Acknowledgements

We are grateful for the financial support given by the National Natural Science Foundation of China for grants (21174080, 21274069, 21334003, and 21422403). The Nankai groups also thanks for Open Research Fund of State Key Laboratory of Polymer Physics and Chemistry, Changchun Institute of Applied Chemistry. Finally, support by the Karlsruhe Nano Micro Facility (KNMF) for the electron microscopic characterization is gratefully acknowledged. We thank Mr. Li-Jun Ren for drawing the scheme of 3D honeycomb structure.

Keywords: Janus co-cluster · nanomaterials · polyoxometalates · self-assembly · silsesquioxanes

How to cite: *Angew. Chem. Int. Ed.* **2015**, *54*, 15699–15704
Angew. Chem. **2015**, *127*, 15925–15930

[1] G. M. Whitesides, J. P. Mathias, C. T. Seto, *Science* **1991**, *254*, 1312–1319.
[2] G. M. Whitesides, B. Grzybowski, *Science* **2002**, *295*, 2418–2421.
[3] J. M. Lehn, *Science* **2002**, *295*, 2400–2403.
[4] C. B. Murray, C. R. Kagan, M. G. Bawendi, *Science* **1995**, *270*, 1335–1338.
[5] A. M. Kalsin, M. Fialkowski, M. Paszewski, S. K. Smoukov, K. J. M. Bishop, B. A. Grzybowski, *Science* **2006**, *312*, 420–424.
[6] M. E. Leunissen, C. G. Christova, A. P. Hynninen, C. P. Royall, A. I. Campbell, A. Imhof, M. Dijkstra, R. van Roij, A. van Blaaderen, *Nature* **2005**, *437*, 235–240.
[7] E. V. Shevchenko, D. V. Talapin, N. A. Kotov, S. O'Brien, C. B. Murray, *Nature* **2006**, *439*, 55–59.
[8] E. V. Shevchenko, D. V. Talapin, C. B. Murray, S. O'Brien, *J. Am. Chem. Soc.* **2006**, *128*, 3620–3637.
[9] D. V. Talapin, J. S. Lee, M. V. Kovalenko, E. V. Shevchenko, *Chem. Rev.* **2010**, *110*, 389–458.
[10] F. S. Bates, G. H. Fredrickson, *Annu. Rev. Phys. Chem.* **1990**, *41*, 525–557.
[11] I. W. Hamley, *The Physics of Block Copolymers*, Oxford University Press, Oxford, **1998**.
[12] M. W. Matsen, M. Schick, *Phys. Rev. Lett.* **1994**, *72*, 2660–2663.

[13] A. K. Khandpur, S. Förster, F. S. Bates, I. W. Hamley, A. J. Ryan, W. Bras, K. Almdal, K. Mortensen, *Macromolecules* **1995**, *28*, 8796 – 8806.
[14] F. S. Bates, M. A. Hillmyer, T. P. Lodge, C. M. Bates, K. T. Delaney, G. H. Fredrickson, *Science* **2012**, *336*, 434 – 440.
[15] H. C. Kim, S. M. Park, W. D. Hinsberg, *Chem. Rev.* **2010**, *110*, 146 – 177.
[16] S. A. Claridge, A. W. Castleman, Jr., S. N. Khanna, C. B. Murray, A. Sen, P. S. Weiss, *ACS Nano* **2009**, *3*, 244 – 255.
[17] X. Roy, C. H. Lee, A. C. Crowther, C. L. Schenck, T. Besara, R. A. Lalancette, T. Siegrist, P. W. Stephens, L. E. Brus, P. Kim, M. L. Steigerwald, C. Nuckolls, *Science* **2013**, *341*, 157 – 160.
[18] A. Turkiewicz, D. W. Paley, T. Besara, G. Elbaz, A. Pinkard, T. Siegrist, X. Roy, *J. Am. Chem. Soc.* **2014**, *136*, 15873 – 15876.
[19] M. Schulz-Dobrick, M. Jansen, *Angew. Chem. Int. Ed.* **2008**, *47*, 2256 – 2259; *Angew. Chem.* **2008**, *120*, 2288 – 2291.
[20] Y. W. Li, W. B. Zhang, I. F. Hsieh, G. L. Zhang, Y. Cao, X. P. Li, C. Wesdemiotis, B. Lotz, H. M. Xiong, S. Z. D. Cheng, *J. Am. Chem. Soc.* **2011**, *133*, 10712 – 10715.
[21] H. Liu, C. H. Hsu, Z. W. Lin, W. P. Shan, J. Wang, J. Jiang, M. J. Huang, B. Lotz, X. F. Yu, W. B. Zhang, K. Yue, S. Z. D. Cheng, *J. Am. Chem. Soc.* **2014**, *136*, 10691 – 10699.
[22] M. J. Huang, C. H. Hsu, J. Wang, S. Mei, X. H. Dong, Y. W. Li, M. X. Li, H. Liu, W. Zhang, T. Aida, W. B. Zhang, K. Yue, S. Z. D. Cheng, *Science* **2015**, *348*, 424 – 428.
[23] M. B. Hu, Z. Y. Hou, Y. Xiao, W. Yu, C. Ma, L. J. Ren, P. Zheng, W. Wang, *Langmuir* **2013**, *29*, 5714 – 5722.
[24] Z. Y. Hou, M. B. Hu, W. Wang, *Acta Chim. Sin.* **2014**, *72*, 61 – 68.
[25] Y. Hou, C. L. Hill, *J. Am. Chem. Soc.* **1993**, *115*, 11823 – 11830.
[26] G. Croce, F. Carniato, M. Milanesio, E. Boccaleri, G. Paul, W. van Beek, L. Marchese, *Phys. Chem. Chem. Phys.* **2009**, *11*, 10087 – 10094.
[27] D. B. Cordes, P. D. Lickiss, F. Rataboul, *Chem. Rev.* **2010**, *110*, 2081 – 2173.
[28] Z. L. Zhang, M. A. Horsch, M. H. Lamm, S. C. Glotzer, *Nano Lett.* **2003**, *3*, 1342 – 1346.
[29] S. C. Glotzer, M. J. Solomon, *Nat. Mater.* **2007**, *6*, 557 – 562.
[30] P. A. Midgley, M. Weyland, *Ultramicroscopy* **2003**, *96*, 413 – 431.
[31] C. Kübel, A. Voigt, R. Schoenmakers, M. Otten, D. Su, T. C. Lee, A. Carlsson, J. Bradley, *Microsc. Microanal.* **2005**, *11*, 378 – 400.
[32] P. A. Midgley, R. E. Dunin-Borkowski, *Nat. Mater.* **2009**, *8*, 271 – 280.
[33] G. van Anders, D. Klotsa, N. K. Ahmed, M. Engel, S. C. Goltzer, *Proc. Natl. Acad. Sci. USA* **2014**, *111*, E4812 – E4821.
[34] R. L. Marson, C. L. Phillips, J. A. Anderson, S. C. Glotzer, *Nano Lett.* **2014**, *14*, 2071 – 2078.
[35] D. Frenkel, *Nat. Mater.* **2015**, *14*, 9 – 12.
[36] CCDC 675452 (Wells–Dawson POM), 206050 (octa-isobutyl-POSS), and 154423 (succinic acid) contain the supplementary crystallographic data for this paper. These data can be obtained free of charge from The Cambridge Crystallographic Data Centre.

Received: August 3, 2015
Revised: October 15, 2015
Published online: November 13, 2015

